J. Electrochem. Sci. Eng. **12(4)** (2022) 651-666; http://dx.doi.org/10.5599/jese.1190

Open Access : : ISSN 1847-9286

https://pub.iapchem.org/ojs/index.php/JESE

Original scientific paper

Mechanical and microstructural characterization of yttria-stabilized zirconia (Y_2O_3/ZrO_2; YSZ) nanoparticles reinforced WC-10Co-4Cr coated turbine steel

Rajinder Kumar[1], Deepak Bhandari[1] and Khushdeep Goyal[2,✉]

[1]*Mechanical Engineering, Yadavindra Department of Engineering, Punjabi University Guru Kashi Campus, Talwandi Sabo, Punjab, India*

[2]*Department of Mechanical Engineering, Punjabi University Patiala, Punjab, India*

Corresponding author: ✉ rkrajinder16@gmail.com

Received: November 26, 2022; Accepted: February 12, 2022; Published: February 24, 2022

Abstract

The aim of this paper is to investigate the WC-10Co-4Cr coatings reinforced with 5 % and 10 % of yttria-stabilized zirconia (Y_2O_3/ZrO_2; YSZ) nanoparticles deposited on the CA6NM turbine steel by using the high-velocity oxy-fuel (HVOF) thermal spraying technique. In the HVOF technique, the hot jet of the semi-solid particles strikes against the workpiece and creates a layer of coating of varying thickness on the substrate material. The coatings fabricated with HVOF were analyzed by scanning electron microscope (SEM) / energy-dispersive x-ray spectroscopy (EDS). The phase identification of a crystalline material was made with the x-ray diffraction (XRD) technique. The mechanical properties in terms of porosity, surface roughness and microhardness of the nanocomposite coatings were also evaluated. The SEM/EDS analysis showed that dense and homogeneous coatings were developed by the reinforcement of YSZ nanoparticles. The peaks of XRD graphs of WC-10Co-4Cr coating reinforced with 5 and 10 % of YSZ nanoparticles revealed that the WC was present as a major phase and W_2C, Co_3W_3C, Co, Co_6W_6C, Co_6W and Y_2O_3/ZrO_2 nanoparticles were observed as a minor phase. The porosity level decreased up to 42 and 56 % by the addition 5 and 10 % of YSZ nanoparticles as compared with conventional WC-10Co-4Cr coating. The surface roughness values for WC-10Co-4Cr conventional coating, 95 % (WC-10Co-4Cr) + 5 % YSZ and 90 % (WC-10Co-4Cr) + 10 % YSZ nanocomposite coated samples were found to be 5.03, 4.89 and 4.28 respectively. The nanocomposite coatings reinforced with 10 % YSZ nanoparticles exhibited the highest microhardness value (1278 HV). The WC-10Co-4Cr coatings reinforced with 10 % of YSZ nanoparticles resulted in low porosity, low surface roughness and high microhardness. During the coating process, the nanoparticles of YSZ flow into the pores and are dispersed in the gaps between the micrometric WC particles and provide a better shield to the

substrate material. The WC-10Co-4Cr with 10 % of YSZ nanoparticles showed better results in terms of mechanical and microstructural properties during the investigation.

Keywords
High velocity oxy fuel (HVOF); mechanical properties; microhardness; nanocomposite coating; porosity

Introduction

Hydroelectric power plants have a significant contribution to power generation. Half of the hydroelectric power resources lie only in the Asian countries [1]. India lies at the seventh position in hydroelectric power production in the world. Due to the increase of sediment content in the water, the problem of erosion becomes more critical during the rainy season and sometimes may cause the major shutdown of these hydroelectric power stations, which causes huge financial loss to the hydropower industry [2]. Major components of the hydro turbines, which are badly eroded, are draft tube, facing plate, runner inlet and outlet, shaft seal, guide vanes, nozzle, spear and spiral casing. Traditional steels used in the manufacturing of hydro turbine components are not able to overcome the problems that occurred due to erosion in the hydroelectric power stations. But different types of surface coatings can be deposited to enhance the life of the materials used in the fabrication of hydro turbine components [3].

Many authors also highlighted that the problem of slurry erosion of hydro turbine components cannot be eliminated, but it can be reduced by using coated components for the hydro turbine. Many researchers compared the conventional coatings with nanostructured coatings and lots of improvements were observed in mechanical and microstructural properties of as-sprayed material as like increase in the microhardness, lower the value of porosity, surface roughness, erosion rate etc. Different types of thermal spray coatings are used daily to resist the erosion wear in various industrial applications such as hydropower plants, thermal power plants and mineral industry. Choy highlighted the utilization of thermal spray processes along with the versatility to spray an extensive variety of materials like composites and ceramics [4]. HVOF spray coatings are used very vastly due to their better mechanical strength, corrosion resistance, erosion resistance, higher value of microhardness, low porosity and improved surface properties of the substrate materials [5,6]. By the application of coatings, the erosion resistance increased and the life of the turbine components was also enhanced [6,7]. To date, many researchers have shown the better mechanical and microstructural properties of the various types of coating deposited by HVOF technique.

From the literature survey, it was observed that the tungsten-based WC-10Co-4Cr coatings are mostly used to resist slurry erosion. Lee *et al.* have observed that the mostly used harder phases are Al, Ni, Cr and Fe, while WC, Si and Al_2O_3 are mainly used as harder binders. The significant improvement was observed in the mechanical properties and the erosion resistance of the target material by applying WC-based coatings [8]. Many researchers like Santa *et al.* and Singh *et al.* applied WC and Cr as the harder materials to control the surface properties of the materials [9,10]. Lee *et al.* examined the surface properties of WC–10Co–4Cr coated stainless steel by using the HVOF technique. The results reveal that stainless steel's wear resistance and bond strength were increased after coating with powders of various particle sizes [8]. Maiti *et al*. studied the effect of WC-based HVOF coatings on the performance of stainless steel 304 by using different compositions of WC-based coatings [11]. Results reveal that the hardness of WC–9Co–5Cr was improved with the addition of 20% WC powder. Hong *et al.* observed the surface properties of Ni–Cr coated 13Cr4Ni steel using the HVOF technique.

It was found that the microhardness of substrate material increased due to the presence of coating composition of different elements [12].

By the addition of chromium, WC-Co-Cr coatings improve the wear resistance, erosion and corrosion as compared to the WC-Co coatings [13]. Investigations showed that the erosion resistance of WC-10Co-4Cr coatings deposited with the HVOF technique increased up to 50% more than substrate stainless steel. The results of WC-based coatings mostly depend on the coating technique [14,15]. Further, the composition of feedstock powders also plays a major role. Chromium carbide coatings enhance the erosion resistance of hydro turbine components [16]. Cermets coatings can be deposited by HVOF, which is a promising technique due to its characteristics [17,18]. The selection of the coating mainly depends on the application; however, the scope of thermal spray coatings has increased vastly in recent years [19,20]. Murthy *et al*. studied HVOF sprayed carbide coatings that have better erosion and wear resistance as compared to D gun spray coatings [21]. The studies of various researchers revealed that the adhesion strength, fracture strength and hardness of the coatings are mainly responsible for the resistance to erosion.

Murthy *et al.* deposited Cr_3C_2-20NiCr and WC-10Co-4Cr on a mild steel material by using the HVOF coating technique [22]. Results revealed that the WC-based coating has a better wear resistance in comparison to the Cr C-based coating due to the high value of hardness of the WC and better bond strength of Co Cr. Additionally, the HVOF coated carbide has excellent wear resistance as compared to other spraying techniques [23]. Goyal *et al.* analyzed the effect of erodent particles on ASTM A743 turbine steel coated with Cr_3C_2-NiCr. They observed that coated steel exhibited brittle behavior, but uncoated steel showed ductility [24].

Kitamura *et al.* studied that Y_2O_3 (yttrium oxide) based coatings performed better than Al_2O_3 (aluminum oxide) based coatings against the erosion resistance [25]. The life span of the various components of the hydro turbine can be increased by depositing nanocomposite coatings on the CA6NM turbine steel material. The major advantage of the HVOF thermal spray technique is that the coatings have low porosity, low surface roughness and high microhardness. There is wide scope of yttria-stabilized zirconia (Y_2O_3/ZrO_2; YSZ) nanoparticles reinforced WC-10Co-4Cr coatings as no more literature exists in this field. In the present research work, the WC-10Co-4Cr reinforced with 5 and 10 % YSZ nanoparticles were deposited on the CA6NM turbine steel by the HVOF technique. The microstructure, different phases of the coatings, porosity, surface roughness, microhardness were investigated using SEM/EDS, X-ray diffraction (XRD), image analyzer software, surface roughness tester, Vickers microhardness tester.

Materials and methods

Substrate material

CA6NM turbine steel material suitable for hydro turbine components was selected for the present investigation. The substrate material (CA6NM turbine steel) was procured from the Atul Precision Cast, Rajkot, Gujarat. The chemical composition of substrate material is reported in Table 1. The samples with dimensions (35×25×5 mm) were prepared from the substrate material to deposit the coatings.

Table 1. *Chemical composition of substrate material (CA6NM turbine steel)*

Element	C	Mn	Cr	Ni	P	Si	Mo	S	Cu	Al	Fe
Content, wt. %	0.018	0.58	12.02	3.63	0.035	0.53	0.76	0.006	0.34	0.005	Rest

Coating powders

The conventional WC-10Co-4Cr coating powder and WC-10Co-4Cr reinforced with varying percentages of YSZ nanoparticles were used for the present investigation. Table 2 shows the coating powders of different coating compositions. To prepare coating powders of different compositions, WC-10Co-4Cr was reinforced with 5 and 10 % of YSZ nanoparticles and rolled continuously for four hours at 200 RPM using RETSCH-Planetary PM-100 low-energy ball mill. The nanocomposite coating powders were prepared to apply on the CA6NM turbine steel to improve the performance and life of turbine components. In the mixture of nanocomposite coating powders, the nanoparticles of YSZ were uniformly dispersed. The presence of blended elements was observed during SEM/EDS analysis.

Table 2. *Composition of coating powders deposited on CA6NM turbine steel samples*

No.	Coating powder content, %	
	Base powder (WC-10Co-4Cr)	Reinforcement, YSZ (Y_2O_3/ZrO_2 nano powder)
1	100	0
2	95	5
3	90	10

Coating technique

The samples of the substrate material were polished using SiC papers of different grit sizes. Then an abrasive blasting machine was used to shoot blast the samples to obtain better bonding between the samples and the coatings. Different nanocomposite feedstock powders were applied on the samples of the substrate material with the HVOF spray coating technique to obtain better bonding with the base material. The different process parameters of HVOF spraying selected for the fabrication of nanocomposite coating are shown in Table 3. After deposition of the nanocomposite coatings, the coatings were cooled with the help of air supplied by air jet.

Table 3. *Process parameters of HVOF used for the fabrication of nanocomposite coating*

Process parameter	Spray distance, mm	Particle size, mm	Flow rate, L min^{-1}			Powder feed rate, $gmin^{-1}$	Pressure, kPa		
			Air	Oxygen	Fuel (LPG)		Fuel	Air	Oxygen
Value	138	15	640	260	75	30	6.2	10	5

Characterization

After the deposition of coatings with the HVOF technique, the samples were cut into the required size (10×10×5 mm) to perform the SEM analysis. SEM analysis was carried out on JEOL (JSM-6510LV) microscope. SEM allows to analyze the grain morphology of the coating powders and coated surface after the deposition of coatings. The SEM provides detailed information about surface characteristics at high magnifications that produce high-resolution images of the coating powders, uncoated, conventionally coated and nanocomposite coated surfaces. Energy dispersive x-ray spectroscopy, also known as EDS analysis, were performed to obtain detailed information about the elemental composition of all samples. X-ray diffraction (XRD) was used for the identification of the crystalline and grains forms known as phases of mixtures present in coating powders, uncoated, conventionally coated and nanocomposite coated surfaces. To investigate the various phases, present in all types of samples, XRD analysis was carried out using PANalytical X'Pert Pro x-ray diffractometer with the copper target (0.15419 nm, 40 kV and 45 mA). Phase identification was made with High Score PLUS software.

Table 4. *Mechanical properties of uncoated and coated samples*

S. No.	Material/coating combination	Porosity, %	Average microhardness, HV	Average surface roughness, µm
1	Uncoated CA6NM Steel	3.402	319	1.59
2	WC-10Co-4Cr	1.942	1088	4.82
3	95 % (WC-10Co-4Cr) + 5 % YSZ	1.131	1257	4.13
4	90 % (WC-10Co-4Cr) +10 % YSZ	0.853	1278	3.45

To observe the porosity of the substrate material, WC-10Co-4Cr conventionally coated sample and WC-10Co-4Cr + YSZ nanocomposite coated samples were cut by wire EDM on either side of the sample for porosity analysis. Measurements of the porosity of the different samples were done with an image analyser, having software of the Envision 3.0 Series (Chennai Metco Private Limited, Chennai, India). The surface roughness of the uncoated and coated samples was measured with the help of a surface roughness tester (Surftest SJ310, Mitutoyo). The microhardness of the substrate material, WC-10Co-4Cr coating and WC-10Co-4Cr + YSZ nanocomposite coatings was measured at a load of 2.942 N using a digital micro vickers hardness tester (SHV-1000, Chennai Metco Private Limited, Chennai).

Results and discussion

SEM/EDS and XRD analysis

Figure 1 shows the surface morphologies of the WC-10Co-4Cr conventional powder, YSZ nanopowder, WC-10Co-4Cr + 5 % YSZ and WC-10Co-4Cr + 10 % YSZ nanocomposite powder. The WC-10Co-4Cr powder is spheroidal in shape and the surface of the powder particles is porous. As seen with high magnification that WC grains are blocky in shape. The density of the YSZ nanopowder is higher than that of the WC-10Co-4Cr conventional powder.

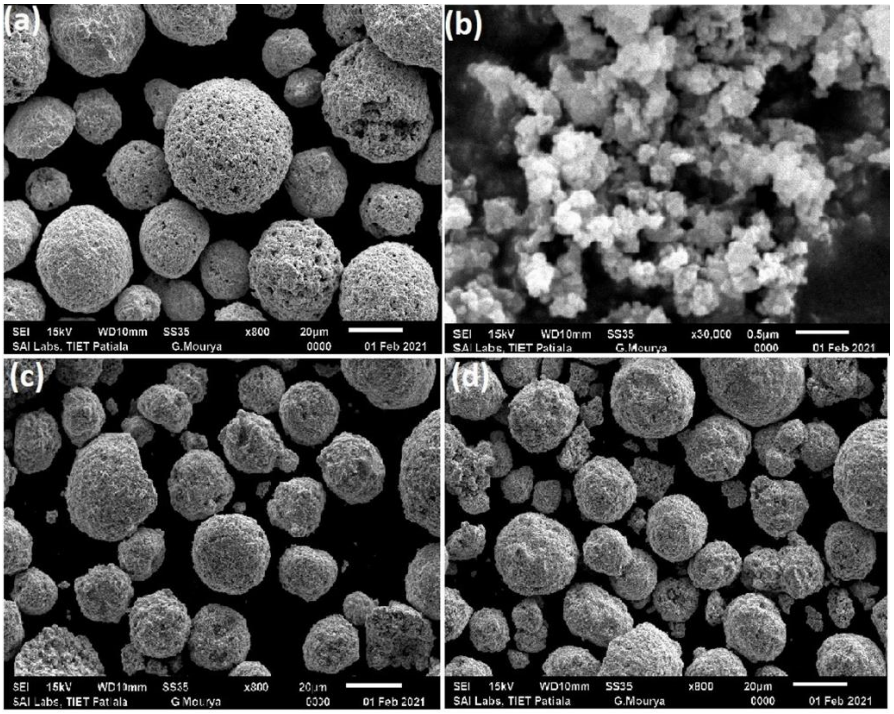

Figure 1. *SEM images of (a)WC-10Co-4Cr conventional powder (b) YSZ nanopowder (c) 95 % (WC-10Co-4Cr) + 5 % YSZ nanocomposite powder (d) 90 % (WC-10Co-4Cr) + 10 % YSZ nanocomposite powder*

The SEM/EDS micrographs of the WC-10Co-4Cr coating powder, as shown in Figure 2, depicted that most of the particles are of spherical shape. It also highlights W is present as a major phase, while Co, Cr and C as a minor phase. After mixing the 5 and 10% of YSZ nanoparticles in WC-10Co-4Cr coating powder using a low-speed ball milling, the SEM/EDS micrographs were taken, as shown in Figure 3 and Figure 4.

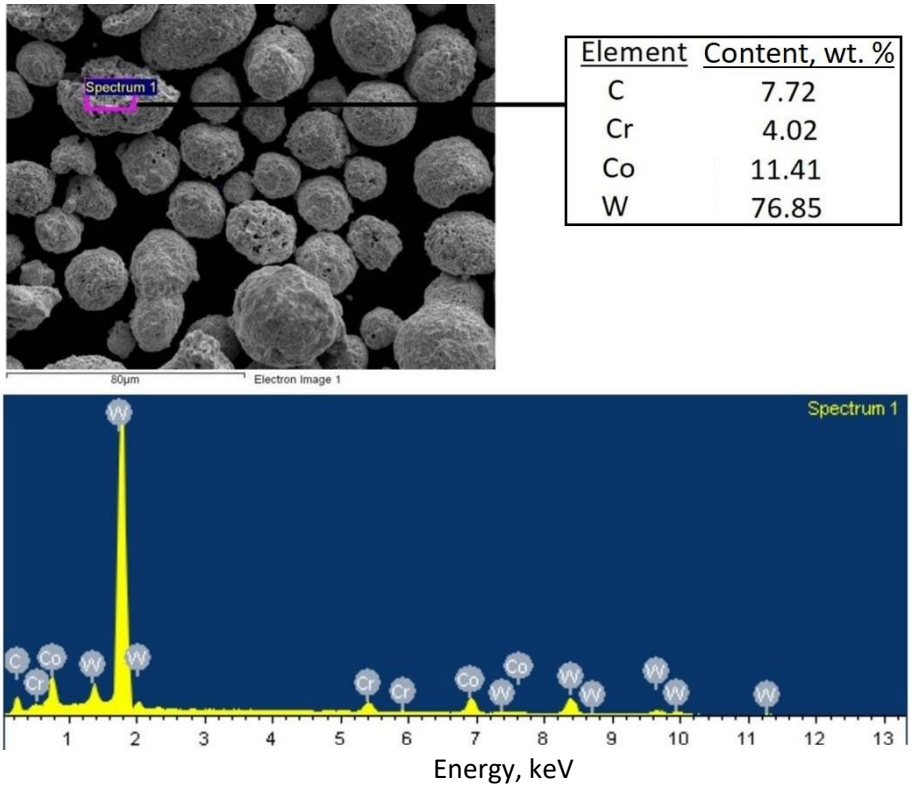

Figure 2. *SEM/EDS micrograph of WC-10Co-4Cr conventional coating powder*

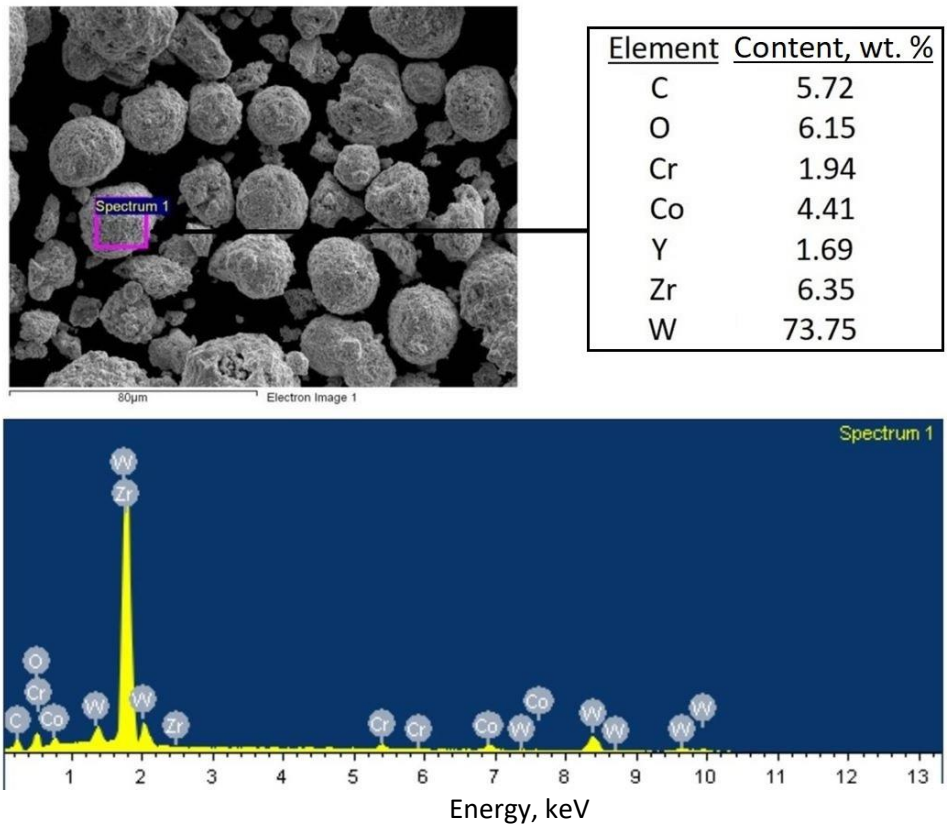

Figure 3. *SEM/EDS micrograph of 95 % (WC-10Co-4Cr) + 5% YSZ nanocomposite coating powder*

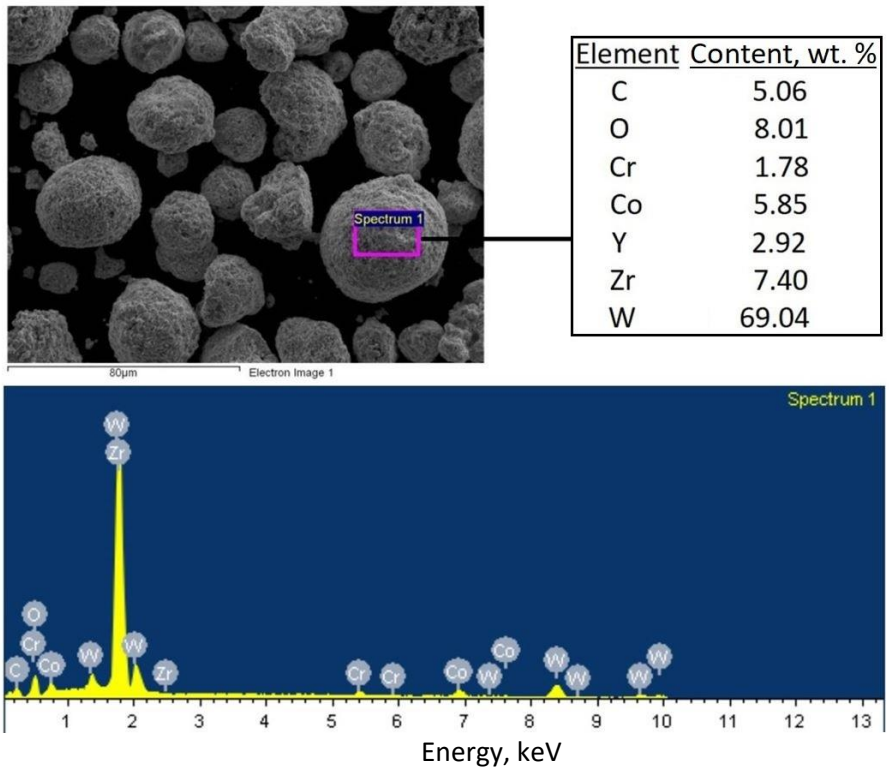

Figure 4.*SEM/EDS micrograph of 90% (WC-10Co-4Cr) + 10 % YSZ nanocomposite coating powder*

These figures clearly show the uniformly dispersed nanoparticles in conventional coating powders. They also exhibited that W, C, O, Co and Zr are present as a major phase while Cr and Y are observed as a minor phase. The YSZ nanoparticles have formed a uniform layer on the outer surface of WC-10Co-4Cr coating powder. The microstructure of HVOF coated samples was also obtained by SEM/EDS surface morphology analysis. Figure 5 shows the surface morphology and composition of the substrate material.

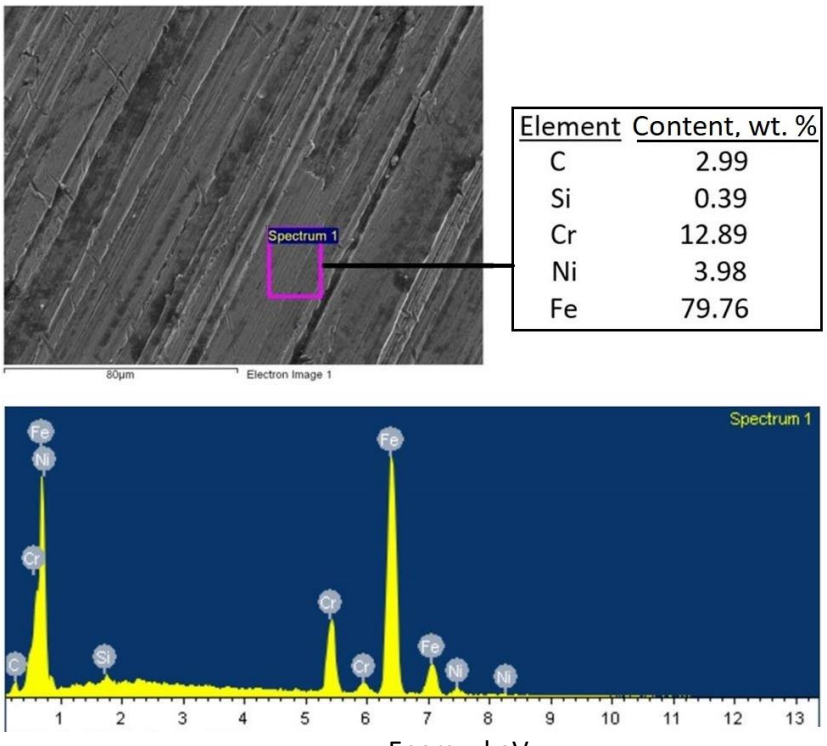

Figure 5. *SEM/EDS micrograph of the CA6NM steel substrate*

The WC-10Co-4Cr coated samples have a uniform, dense structure, as shown in Figure 6. Some un-burnt particles were seen on the coated surface. The figure also revealed that the Cr, C, O and Ni are present in more percentage. Figure 7 and Figure 8 showed the SEM images of WC-10Co-4Cr + 5 % YSZ and WC-10Co-4Cr + 10 % YSZ nanocomposite coatings. The dense and uniform layer of coating was obtained by the reinforcement of nanoparticles of YSZ. The Cr, O and C are observed as a major phase.

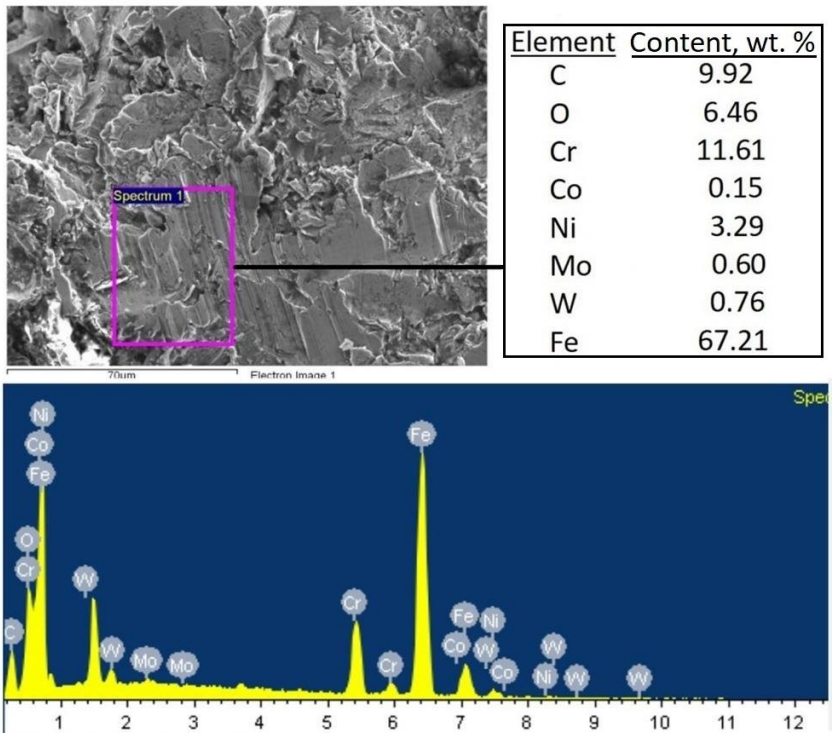

Figure 6. *SEM/EDS micrograph of WC-10Co-4Cr coated sample*

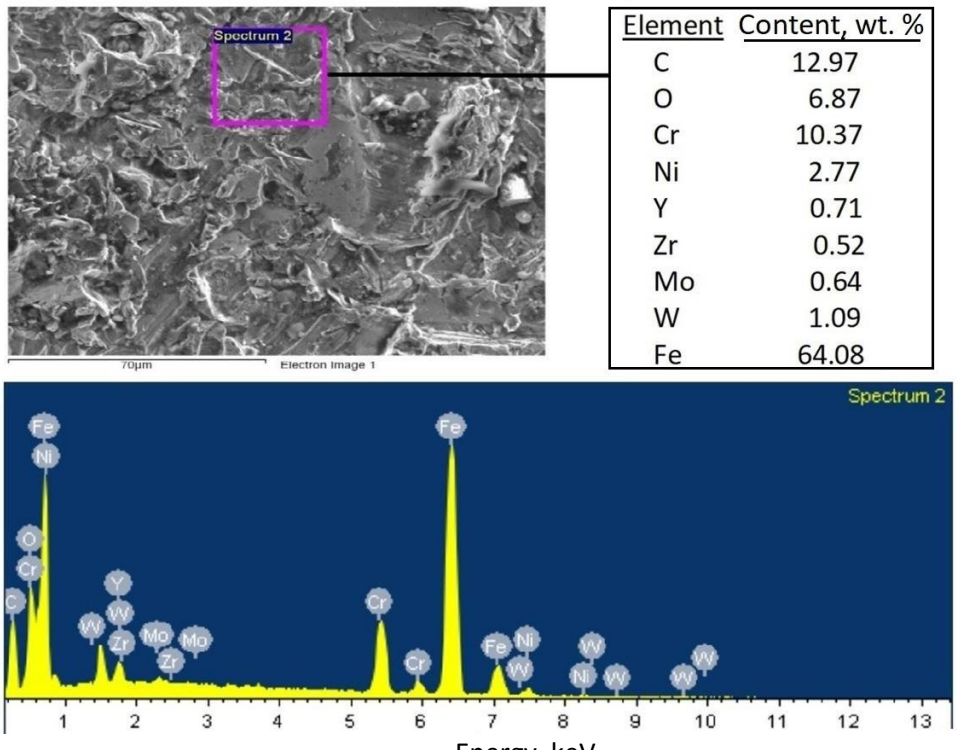

Figure 7. *SEM/EDS micrograph of 95 % (WC-10Co-4Cr) + 5 % YSZ nanocomposite coated sample*

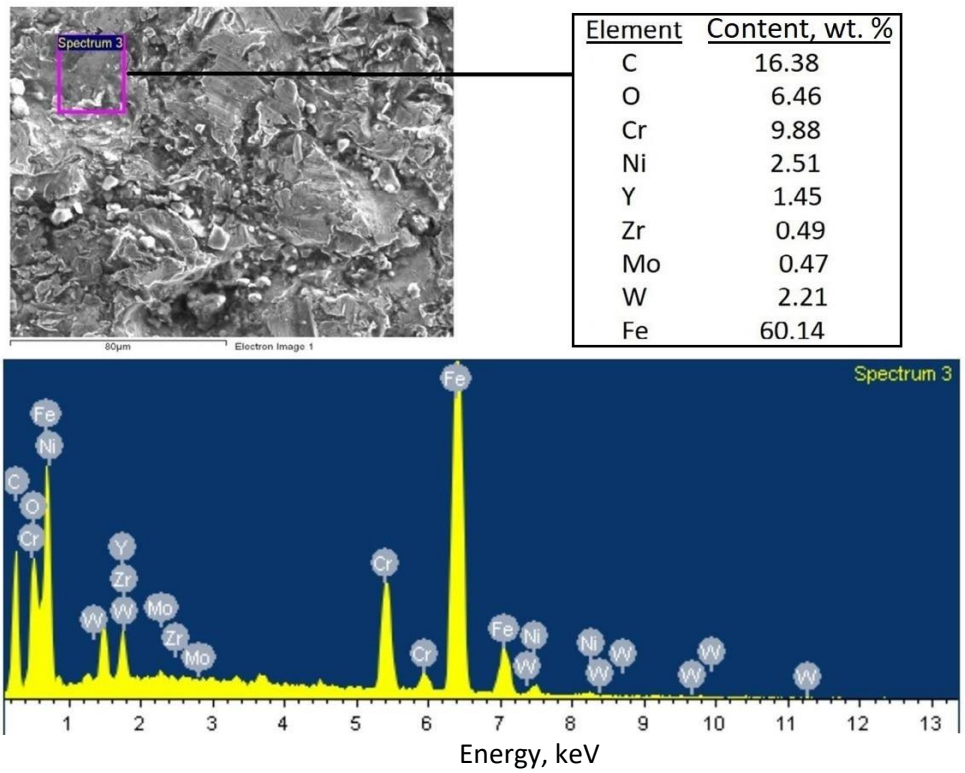

Figure 8. *SEM/EDS micrograph of 90 % (WC-10Co-4Cr) + 10 % YSZ nanocomposite coated sample*

The oxide formation was reduced as the nanoparticles of YSZ filled the porous gaps. It was also analyzed by SEM/EDS that the nanoparticles of YSZ are well dispersed in WC-10Co-4Cr coating powders, which are responsible for decreasing the porosity and surface roughness of the nanocomposite coatings.

The XRD tests were performed on the substrate material, traditional coating of WC-10Co-4Cr and nanocomposite coatings of WC-10Co-4Cr with 5 and 10 % of YSZ nanoparticles. The XRD pattern for WC-10Co-4Cr coated surface, as shown in Figure 9(a), presented the peaks corresponding to WC, W_2C, Co_3W_3C, and Co phases. WC was identified as the major phase present in the coating. Further W_2C, Co_3W_3C phases were also present due to the decarburization of WC particles. Co was also identified from the XRD diffraction pattern. It is in good agreement with the observations made by other researchers [26,27]. The transformation of WC to W_2C on the surface of WC particles occurred due to the direct oxidation of solid WC [28,29]. Figures 9(b) and 9(c) represent the results of the XRD analysis of WC-10Co-4Cr coatings reinforced with 5 and 10 % of YSZ nanoparticles. The XRD pattern in the figures reveals the presence of WC, W_2C, Co_6W_6C, Co_6W and Y_2O_3/ZrO_2crystalline phases. The WC was observed as the major phase followed by CO_6W_6C. Similar trends have been reported by the other authors [30-32]. The existence of Co_6W is owing to the reaction of WC particles slightly melted in the bond phase Co–Cr during solid-state sintering. The diffraction peaks of the Co phase disappear owing to the formation of the amorphous phase by rapid cooling. The peaks of the Co_6W_6C phase are observed in both nanocomposite coatings because of the dissolution of WC in the cobalt matrix. The XRD peaks corresponding to Y_2O_3/ZrO_2 indicate that the YSZ nanoparticles are dispersed in the gaps between the micrometric WC particles or partially agglomerated in the bonding phase. The XRD patterns depicted that the HVOF method can effectively limit the generation of decarburization phases because of the high velocity and relatively low temperature of the flame. The increase in the formation of non-crystalline amorphous phases occurs due to very fast cooling during the spraying process [33]. Stewart *et al.* demonstrated that the presence of different phases and their proportion

mostly depends on the process conditions when depositing the coating powder on the base material [34].

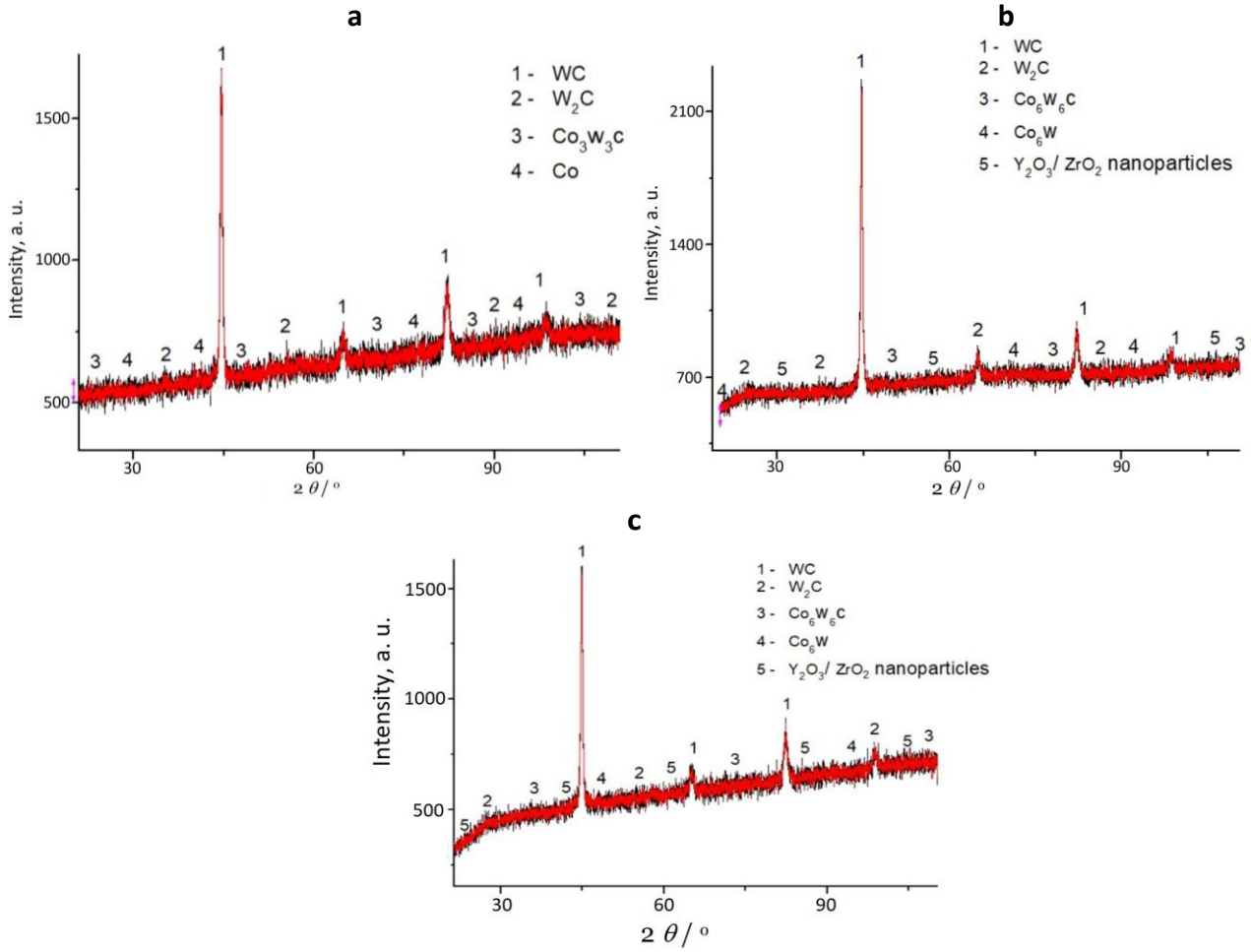

Figure 9. *XRD images of (a) WC-10Co-4Cr coated sample (b) 95 % (WC-10Co-4Cr) +5 % YSZ nanocomposite coated sample(c) 90 % (WC-10Co-4Cr) + 10 % YSZ nanocomposite coated sample*

Figure 10(a) shows the microstructure of the cross-section of uncoated CA6NM steel. Pores were observed in the substrate material, resulting in low microhardness and high porosity. Figure 10(b) shows the small voids and pores in the cross-sectional microstructure of the WC-10Co-4Cr coated sample. Dense grains were observed in the cross-sectional microstructure of nanocomposite coating of WC-10Co-4Cr + 5 % YSZ and WC-10Co-4Cr + 10 % YSZ as presented in Figure 10(c) and Figure 10(d). The material spreads uniformly on the surface and forms a more homogeneous layer as the YSZ nanoparticles fill the pores in the coatings. Minor imperfections were observed in the cross-sectional microstructure of nanocomposite coating of WC-10Co-4Cr + 10% YSZ, as shown in Figure 10(d).

Figure 11(a) shows the morphological characteristics of the substrate material. Dense grains were observed in the substrate material, due to which material spreads uniformly on the surface and forms the more homogeneous layer. Some imperfections and protrusions in the WC-10Co-4Cr coated surface as shown in Figure 11(b). Goyal et al. also observed that protrusions were formed due to improper melting of ceramic particles before sticking with base metal during the HVOF coating process [35]. The microstructure of nanocomposite coating of WC-10Co-4Cr + 5 % YSZ showed delamination, unmelted nanoparticles of Y_2O_3/ZrO_2, small pores and a layer with lamellar structure, containing a discrete oxide film in their outline, which is the common feature of HVOF coatings as presented in Figure 11(c).

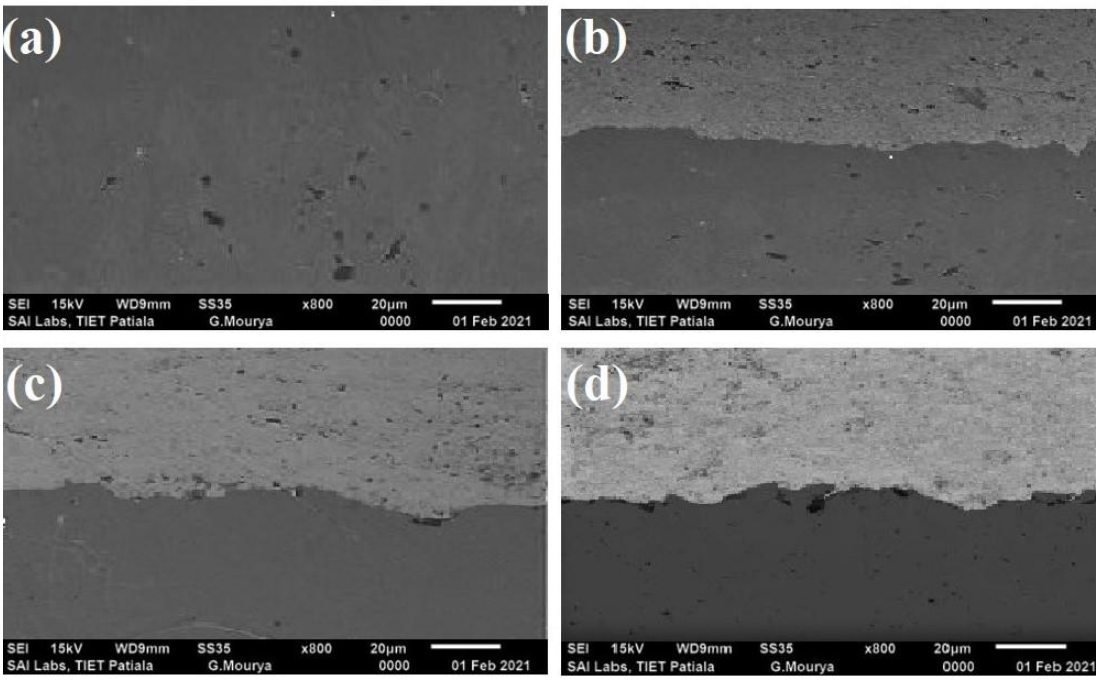

Figure 10. *Microstructure of the cross-section of (a) uncoated CA6NM steel; (b) WC-10Co-4Cr coated sample (c) 95 % (WC-10Co-4Cr) + 5 % YSZ nanocomposite coated sample; (d) 90 % (WC-10Co-4Cr) + 10 % YSZ nanocomposite coated sample*

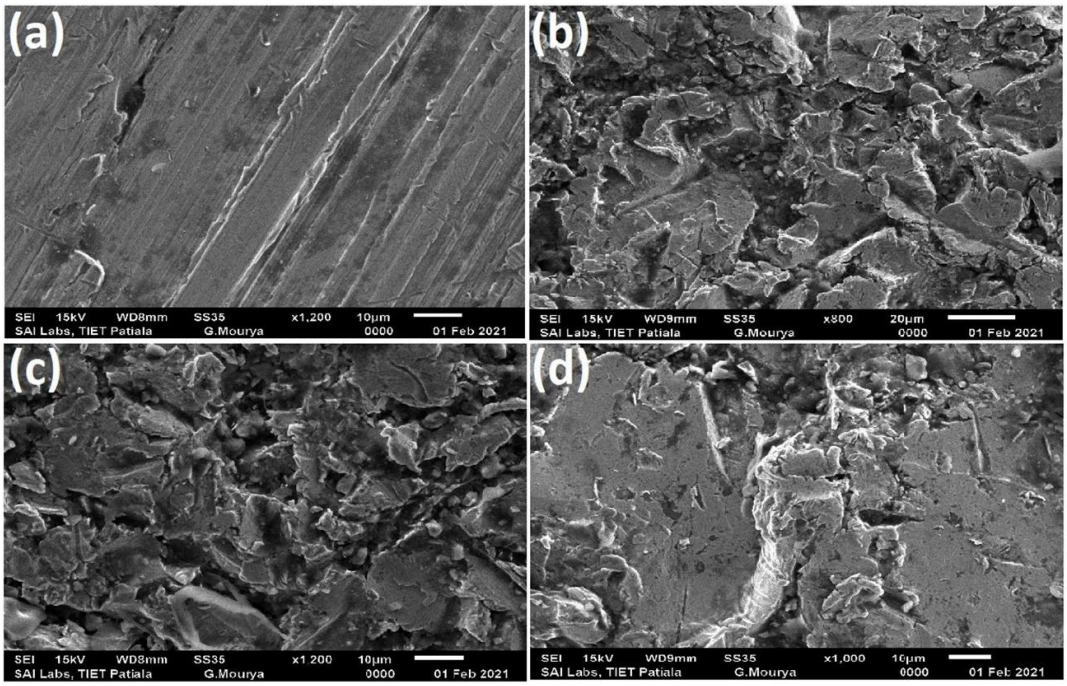

Figure 11. *SEM images of (a) uncoated CA6NM steel (b) WC-10Co-4Cr coated sample (c) 95 % (WC-10Co-4Cr) + 5 % YSZ nanocomposite coated sample (d) 90 % (WC-10Co-4Cr) + 10 % YSZ nanocomposite coated sample*

These features are appeared due to the overlapping of high-speed melt and semi-fused particles deposited on the base material [36]. As the YSZ nanoparticles fill the pores in the coatings, only minor imperfections were observed in the microstructure of nanocomposite coating of WC-10Co-4Cr + 10 % YSZ as shown in Figure 11(d). These types of coatings have dense grains, which create a more homogeneous layer because material spreads more uniformly over the surface. Also, this type of surface morphology is desirable for the HVOF coating process, as it allows the better flow of the

coating powder in the spray gun during the deposition of the coating [37-39]. Thus, WC-10Co-4Cr + 10 % YSZ nanocomposite coating performed better than the other coatings mentioned. The mixing of coating powders improved the microstructure of the coating, attributed to the decrease in process temperature during HVOF coating [40]. Ramesh *et al.* and Rao *et al.* studied that lower porosity and higher microhardness of the coating were exhibited due to the dense laminar structure of the coating along with higher cohesive strength [41-43].

Porosity and surface roughness analysis

The porosity of the coatings was measured at the as polished cross-section of the samples. The apparent porosity values for the substrate material, WC-10Co-4Cr conventional coating, 95 % (WC-10Co-4Cr) + 5 % YSZ and 90 % (WC-10Co-4Cr) + 10 % YSZ nanocomposite coatings were observed as 3.040, 1.942, 1.131 and 0.853 %. Table 4 shows that the porosity decreases with an increase in the percentage of nanoparticles of YSZ in the conventional coating powder. The porosity of the nanocomposite coatings was decreased as the nanoparticles of YSZ filled the pores and interlocked the grains of the coating matrix. The maximum decrease of the porosity level 0.853 % was observed for 90% (WC-10Co-4Cr) + 10 % YSZ nanocomposite coating. The surface roughness values for uncoated and coated samples are also given in Table 4. Improvements were observed by the addition of the nanoparticles of YSZ in the WC-10Co-4Cr coating powder. The surface roughness values for WC-10Co-4Cr conventional coating, 95 % (WC-10Co-4Cr) + 5 % YSZ and 90 % (WC-10Co-4Cr) + 10 % YSZ nanocomposite coated samples were found to be 4.82, 4.13 and 3.45 respectively. Better surface characteristics were observed for 90 % (WC-10Co-4Cr) + 10 % YSZ nanocomposite coating as compared to conventional WC-10Co-4Cr coating as the surface roughness was decreased by the addition of YSZ nanoparticles. The lower value of the porosity for 90 % (WC-10Co-4Cr) + 10 % YSZ nanocomposite coating is the main reason for decreasing the surface roughness. Porosity is one of the major coating characteristics that greatly affect the coating properties. Manjunatha *et al*. studied that carbon nanotubes reinforced HVOF coating resulted in low porosity as the carbon nanoparticles fill the voids in the coatings and improve the bond strength of the coatings [44]. Goyal and Goyal studied that the coatings of Cr_3C_2–20NiCr reinforced with carbon nanotubes exhibited a decrease in the porosity of the coating. Carbon nanotubes interlocked the particles of Cr_3C_2–20NiCr and provided resistance to the surface against eroding particles [45].

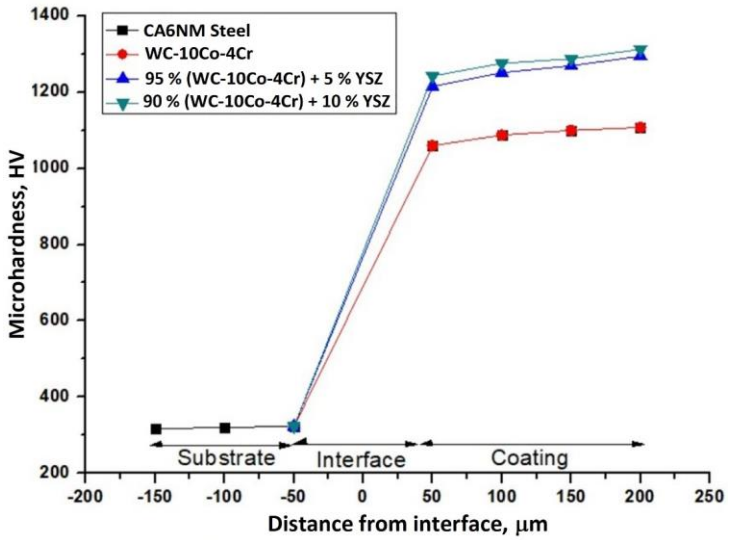

Figure12. *Microhardness profile for substrate material and coated samples*

Vickers micro-hardness

The variation of microhardness along the cross-section of coated substrate material is shown in Figure 7. There is a substantial increase in the microhardness from the substrate to the coating. The average microhardness values of substrate material, WC-10Co-4Cr conventional coating, 95 % (WC-10Co-4Cr) + 5 % YSZ and 90 % (WC-10Co-4Cr) + 10 % YSZ nanocomposite coatings were found to be in the range of 320 HV, 1088 HV, 1257 HV, and 1278 HV respectively as reported in Table 4. The reinforcement of YSZ nanoparticles in the coatings helps to reduce the voids and pores between the coating matrix, thereby decreasing porosity and increasing the microhardness of the nanocomposite coatings. The increase in slurry erosion resistance of coated materials can be attributed to the increase in the microhardness of the coatings [42,35]. Singh *et al.* analysed the erosion tribo performance of WC-10Co-4Cr and WC-10Co-4Cr + 2 % Y_2O_3 deposited on pump impeller steel by HVOF. Results showed that the reinforcement of 2 % Y_2O_3 in WC-10Co-4Cr has increased the erosion wear resistance as the hardness of the substrate material increases from 1130 HV to 1190 HV [46]. The presence of different phases in the SEM images is mainly responsible for the variation in microhardness values.

With the addition of 5% and 10 % of the YSZ nanoparticles in the WC-10Co-4Cr, the surface roughness and porosity were reduced significantly. The porosity decreased up to 42 and 56 % and the surface roughness was reduced up to 15 and 28 % by the reinforcement of 5 and 10 % of the YSZ nanoparticles, respectively, compared to conventional WC-10Co-4Cr coating. Nanoparticles of YSZ interlocked the WC-10Co-4Cr grains and filled the pores in the nanocomposite coating matrix, which resulted in a decrease in surface roughness and porosity. The decrease in porosity with the reinforcement of nanoparticles in the conventional coatings has also been observed by various researchers [47-51]. Reduction in the surface roughness and porosity resulted in the increase in the microhardness of the WC-10Co-4Cr nanocomposite coatings as compared to conventional coating. Indentation resistance was enhanced due to the reinforcement of nanoparticles of YSZ in the WC-10Co-4Cr. Enhanced melting due to the higher thermal conductivity of YSZ nanoparticles resulted in better adhesion with the substrate material and increased microhardness of the WC-10Co-4Cr nanocomposite coatings. Therefore, based on the result and discussion, it was reported that the WC-10Co-4Cr + YSZ nanocomposite coatings are able to enhance the microstructural and mechanical properties of turbine steel.

Conclusion

The experimental analysis conducted on the nanocomposite coating concluded as given below:

The SEM/EDS analysis revealed that the reinforcement of YSZ nanoparticles developed dense and homogeneous coatings. It was also analyzed by SEM/EDS that the nanoparticles of YSZ is well dispersed in WC-10Co-4Cr coating powders, which are responsible for decreasing the porosity and surface roughness of the nanocomposite coatings.

The XRD peaks of WC-10Co-4Cr coatings reinforced with 5 and 10 % of YSZ nanoparticles revealed that the WC was present as a major phase and W_2C, Co_6W_6C, Co_6W and Y_2O_3/ZrO_2 nanoparticles were observed as a minor phase. The XRD peaks corresponding to Y_2O_3/ZrO_2 indicate that the YSZ nanoparticles are dispersed in the gaps between the micrometric WC particles.

For the coated samples, the porosity values were found as 1.942, 1.131 and 0.853 % and the porosity decreased up to 42 and 56 % by the addition of YSZ nanoparticles compared with conventional WC-10Co-4Cr coating. The maximum decrease of 0.853 % of porosity was

obtained for the nanocomposite coating reinforced with 10% YSZ nanoparticles. The surface roughness values for WC-10Co-4Cr conventional coating, 95 % (WC-10Co-4Cr) + 5 % YSZ and 90 % (WC-10Co-4Cr) + 10 % YSZ nanocomposite coatings were found to be 4.82, 4.13 and 3.45 respectively. The surface roughness was improved up to 15 and 28 % by reinforcing 5 and 10 % of the YSZ nanoparticles.

The average microhardness for the coated samples was found to be 1088 HV, 1257HV, and 1278 HV, respectively. The nanocomposite coatings reinforced with 10 % YSZ nanoparticles exhibited the highest microhardness value (1278 HV) and low value of porosity and surface roughness. The YSZ nanoparticles fill the porous gaps, resulting in the increase of bond strength as well as the microhardness of the nanocomposite coatings.

The microstructure of nanocomposite coating of 90 % (WC-10Co-4Cr) + 10 % YSZ showed improved surface morphology. These coatings have dense grains, which create a more homogeneous layer because material spreads more uniformly over the surface.

The present analysis revealed that the reinforcement of YSZ nanoparticles in the conventional coating improved the bonding at the interface of the substrate base and the coatings. Therefore, it is concluded that the CA6NM turbine steel coated with 90 % (WC-10Co-4Cr) + 10 % YSZ exhibited better microstructural and mechanical properties.

References

[1] O. Edenhofer, M. R. Pichs, Y. P. Sokona, *Special report of the intergovernmental panel on climate change* Cambridge University Press New York (2011). ISBN 978-1-107-02340-6

[2] H. Kumar, C. Chittosiya, V. N. Shukla, *Science Direct Material Today* **5** (2018) 6413-6420. https://doi.org/10.1016/j.matpr.2017.12.253

[3] R. Kumar, D. Bhandari, K. Goyal, *IOP Conference Series: Materials Science and Engineering* **1033** (2021) 012064. https://doi.org/10.1088/1757-899X/1033/1/012064

[4] K. L. Choy, *Progress in Materials Science* **48(2)** (2003) 157-170. https://doi.org/10.1016/S0079-6425(01)00009-3

[5] V. Javaheri, D. Porter, V. T. Kuokkala, *Wear* **408-409** (2018) 248-273. https://doi.org/10.1016/j.wear.2018.05.010

[6] M. A. Bukhaiti, S. M. Ahmed, F. M. F. Badran, K. M. Emara, *Wear* **262(9-10)** (2007) 1187-1198. https://doi.org/10.1016/j.wear.2006.11.018

[7] H. Singh, K. Goyal, D. K. Goyal, *Transactions of the Indian Institute of Metals* **70(6)** (2016) 1585-1592. https://doi.org/10.1007/s12666-016-0956-y

[8] C. W. Lee, J. H. Han, J. Yoon, M. C. Shin, S. I. Kwun, *Surface and Coating Technology* **204(14)** (2010) 2223–2229. https://doi.org/10.1016/j.surfcoat.2009.12.014

[9] J. F. Santa, L. A. Espitia, J. A. Blanco, S. A. Romo, A. Toro, *Wear* **267(1-4)** (2009) 160-167. https://doi.org/10.1016/j.wear.2009.01.018

[10] J. P. Singh, S. Kumar, S. K. Mohapatra, *Wear* **376-377** (2017) 1105-1111. https://doi.org/10.1016/j.wear.2017.01.032

[11] A. K. Maiti, N. Mukhopadhyay, R. Raman, *Surface and Coating Technology* **201(18)** (2007) 7781-7788. https://doi.org/10.1016/j.surfcoat.2007.03.014

[12] S. Hong, Y. Wu, Q. Wang, G. Ying, G. Li, W. Gao, B. Wang, W. Guo, *Surface and Coating Technology* **225** (2013) 85-91. https://doi.org/10.1016/j.surfcoat.2013.03.020

[13] A. Kumar, A. Sharma, S. K. Goel, *Applied Surface Science* **370** (2016) 418-426. https://doi.org/10.1016/j.apsusc.2016.02.163

[14] M. F. Ashby, D. R. H. Jones, *Engineering Materials 2,* Pergamon Press, Oxford (2006). ISBN 978-0-08-0096668-7

[15] H. Skuleva, S. Malinovb, W. Shac, P. A. M. Basheer, *Surface and Coating Technology* **197** (2005) 177-184. http://doi.org/10.1016/j.surfcoat.2005.01.039
[16] K. Goyal, *World Journal of Engineering* **16(1)** (2019) 64-70. https://doi.org/10.1108/ WJE-08-2018-0262
[17] I. E. Celik, O. Culha, B. Uyulgan, N. F. Akazem, I. Ozdemir, A. Turk, *Surface and Coating Technology* **200(14-15)** (2006) 4320-4328. https://doi.org/10.1016/j.surfcoat.2005.02.158
[18] H. Vasudev, G. Prashar, L. Thakur, A. Bansal, *Surface Topography: Metrology and Properties* **9(3)** (2021) 035003. https://doi.org/10.1088/2051-672X/ac1044
[19] S. Luyckx, C. N. Machio, *International Journal of Refractory Metals and Hard Materials* **25** (2007) 11-15. https://doi.org/10.1016/j.ijrmhm.2005. 10.009
[20] S. Hong, Y. Wu, J. Zhang, *Ultrasonics Sonochemistry* **31** (2016) 563–-569. https://doi.org/10.1016/j.ultsonch.2016.02.011
[21] J. K. N. Murthy, D. S. Rao, B. Venkataraman, *Wear* **249(7)** (2001) 592-600. https://doi.org/10.1016/S0043-1648(01)00682-2
[22] J. K. N. Murthy, B. Venkataraman, *Surface and Coating Technology* **200(8)** (2006) 2642-2652. https://doi.org/10.1016/j.surfcoat.2004.10.136
[23] D. Mahmoudi, A. T. Tabrizi, H. Aghajani, *Surface Topography: Metrology and Properties* **9(1)** (2021) 015025. https://doi.org/10.1088/2051-672X/abe6f3
[24] D. K. Goyal, H. Singh, H. Kumar, V. Sahni, *Journal of Tribology* **136(4)** (2014) 041602. https://doi.org/10.1115/1.4027621
[25] J. Kitamura, Z. Tang, H. Mizuno, K. Sato, A. Burgess, *Journal of Thermal Spray Technology* **20(1-2)** (2011) 170–185. https://doi.org/10.1016/S1359-6454(99)00440-1
[26] D. A. Stewart, P. H. Shipway, D. G. McCartney, *Acta Materialia* **48** (2000) 1593-1604. https://doi.org/10.1016/S1359-6454(99)00440-1
[27] T. Sudaprasert, P. H. Shipway, D. G. McCartney, *Wear* **255** (2003) 943-949. https://doi.org/10.1016/S0043-1648(03)00293-X
[28] J. Subrahmanyam, M. P. Srivastava, R. Sivakumar, *Materials Science and Engineering* **84** (1986) 209-214. https://doi.org/10.1016/0025-5416(86)90240-5
[29] W. Coulson, S. J. Harris, *Transactions of the Institute of Metal Finishing***75** (1997) 108–112. https://doi.org/10.1080/00202967.1997.11871153
[30] J. Barber, B. G. Mellor, R. J. K. Wood, *Wear* **259(1)** (2005) 125-134. https://doi.org/10.1016/j.wear.2005.02.008
[31] Y. Xie, X. Pei, S. Wei, *International Journal of Surface Science and Engineering***10(4)** (2016) 365-374. https://dx.doi.org/10.1504/IJSURFSE.2016.077536
[32] I. Hussainova, J. Kubarsepp, J. Pirso, *Wear* **250(1-12)** (2001) 818–825. http://dx.doi.org/10.1016/S0043-1648(01)00737-2
[33] W. Zhang, C. Ji, Q. Fu, Z. Shi, *Surface Topography: Metrology and Properties* **8(3)** (2020) 035014. https://doi.org/10.1088/2051-672X/abb294
[34] D. A. Stewart, P.H. Shipway, D. G. McCartney, *Wear* **225(2)** (1999) 789-798. https://doi.org/10.1016/S0043-1648(99)00032-0
[35] D. K. Goyal, H. Singh, H. Kumar, V. Sahni, *Journal of Thermal Spray Technology* **21** (2012) 838-851. https://doi.org/10.1007/s11666-012-9795-5
[36] C. Zhang, Z. Jiang, L. Zhao, Surface Topography: *Metrology and Properties* **8(3)** (2020) 035010. https://doi.org/10.1088/2051-672X/abade5
[37] L. Thakur, N. Arora, *Surface and Coating Technology* **309** (2017) 860-871. https://doi.org/10.1016/j.surfcoat.2016.10.073
[38] N. Francis, K. Viswanadhan, M. Paulose, *Materials and Manufacturing Process* **31(7)** (2016) 969-975. https://doi.org/10.1080/10426914.2015.1090585

[39] H. Arabnejad, A. Mansouri, S. Shirazi, B. McLaury, *Wear* **332** (2015) 1044-1050. https://doi.org/10.1016/j.wear.2015.01.031
[40] P. Fauchais, M. Vardelle, A. Vardelle, S. Goutier, *Sprays Used for Thermal Barrier* Coatings in *Droplet and Spray Transport: Paradigms and Applications*, S. Basu, A. Kumar Agarwal, A. Mukhopadhyay, C. Patel, Eds., Springer (2018) 311-344. https://doi.org/10.1007/978-981-10-7233-8_12
[41] M. Ramesh, S. Prakash, S. Nath, P.K. Sapra, B. Venkataraman, *Wear* **269(3)** (2010) 197-205. https://doi.org/10.1016/j.wear.2010.03.019
[42] K. V. S. Rao, K. Girisha, S. Eswar, *Material Today Proceeding* **4(9)** (2017) 10221-10224. https://doi.org/10.1016/j.matpr.2017.06.352
[43] K. Goyal, *Tribology – Materials, Surfaces and Interfaces* (2018) 97-106. https://doi.org/10.1080/17515831.2018.1452369
[44] K. Manjunathaa, G. Giridhara, N. Jegadeeswaran, *Material Today Proceeding* **45(1)** (2021) 15-20. https://doi.org/10.1016/j.matpr.2020.09.219
[45] K. Goyal, R. Goyal, *Surface Engineering* **36(11)** (2020) 1200-1209 https://doi.org/10.1080/02670844.2019.1662645
[46] G. Singh, S. Kumar, S. S. Sehgal, *Particulate Science and Technology* **38(1)** (2020) 34-44. https://doi.org/10.1080/02726351.2018.1501780
[47] H. Asgari, G. Saha, M. Mohammadi, *Journal of Material Science and Technol*ogy **43** (2017) 2123-2135. https://doi.org/10.1016/j.ceramint.2016.10.193
[48] Y. Mazaheri, F. Karimzadeh, M. H. Enayati, *Journal of Material Science and Technol*ogy **29** (2013) 813-820. https://doi.org/10.1016/j.jmst.2013.05.019
[49] Y. Huang, X. Ding, C. Q. Yuan, Z. K. Yu, Z. X. Ding, *Triobology International* **148** (2020) 106315. https://doi.org/10.1016/j.triboint.2020.106315
[50] V. Sharma, M. Kaur, S. Bhandari, *Engineering Research Express* **1(1)** (2019) 012001. https://doi.org/10.1088/2631-8695/ab3cfb
[51] E. Turunen, T. Varis, T. W. Gustafsson, J. Keskinen, *Surface and Coating Technology* **200** (2006) 4987-4994. https://doi.org/10.1016/j.surfcoat.2005.05.018